



# The height of the maximum ionospheric electron density over the MU radar

Shun-Rong Zhang<sup>a, b, \*</sup>, Shoichiro Fukao<sup>a</sup>, William L. Oliver<sup>c</sup>, Yuichi Otsuka<sup>a</sup>

<sup>a</sup>Radio Atmospheric Science Center, Kyoto University, Uji, Kyoto 611-0011, Japan

<sup>b</sup>Wuhan Institute of Physics and Mathematics, CAS, PO Box 71010, Wuhan 430071, People's Republic of China

<sup>c</sup>Department of Electrical and Computer Engineering and Center for Space Physics, Boston University, Boston, MA 02215, USA

Received 27 April 1999; received in revised form 7 September 1999; accepted 20 October 1999

---

## Abstract

Ionospheric  $F_2$ -layer peak height  $h_m F_2$  variations, as measured over 1986–1995 by the MU radar (34.85°N, 136.1°E) and as calculated with a theoretical model, are discussed. The diurnal variations of the measured peak height for different seasons and levels of solar activity are compared with those estimated from ionosonde  $M3000F_2$  and IRI predictions. Also given are the measured ion drift velocities and meridional neutral winds needed to understand the dynamic behavior of the  $F_2$ -layer. It is found that: (1)  $h_m F_2$  is generally higher during periods of the solar maximum than during periods of the solar minimum, and higher in summer than in winter; (2) for the solar maximum,  $h_m F_2$  drops markedly in the morning and in the afternoon, while, for the solar minimum, the  $h_m F_2$  minimum occurs in the morning during summer and usually in the afternoon during winter. In general, the measured  $h_m F_2$  is well reproduced by our model when we use the observed drift velocities and plasma temperatures as inputs. Our modeling study shows that the neutral wind contributes strongly to the diurnal variation of  $h_m F_2$  in winter by lowering the ionization layer by day, particularly for the solar maximum; it also helps to enlarge the day–night difference of  $h_m F_2$  in summer. The northward electromagnetic drifts that usually cancel the neutral wind effect have only a minor effect for the location of the MU radar. Other features of the observed  $h_m F_2$  variations, e.g., the solar maximum–minimum difference, the summer–winter difference, and the morning and afternoon drops, are explained by the basic processes of  $O^+$  production, loss and diffusion, as influenced by the atomic oxygen concentration and neutral and plasma temperatures. © 2000 Elsevier Science Ltd. All rights reserved.

---

## 1. Introduction

The ionospheric  $F_2$ -layer electron density peak is established essentially as a result of the combined effects of two principal ionospheric processes:  $O^+$  loss and diffusion (see, e.g., Rishbeth and Garriott, 1969).

In the bottomside of the  $F$  layer the  $O^+$  concentration increases with increasing altitude during the daytime because the concentrations of  $N_2$  and  $O_2$ , to which  $O^+$  is lost, decrease more rapidly with increasing altitude than does the concentration of  $O$ , from which  $O^+$  is produced. At night, the  $O^+$  concentration similarly decreases with decreasing altitude into the bottomside as the ionospheric plasma remaining from day-time production diffuses downward and is lost to the  $N_2$  and  $O_2$  below. At higher altitudes, owing to the reduced chance of collisions with neutral particles,  $O^+$

---

\* Corresponding author. Present address: Center for Space Physics, Boston University, Boston, MA 02215, USA.

E-mail address: shunrong@bu.edu (S.R. Zhang).

comes under strong diffusion control and so decreases in concentration exponentially with increasing altitude. A density peak is therefore established at an altitude  $h_m F_2$  near the level at which loss and diffusion are of comparable importance. A vertical plasma drift, induced by neutral winds or electric fields, alters  $h_m F_2$  such that an equatorward wind elevates the ionization along the geomagnetic field lines to a region in which  $N_2$  and  $O_2$  are even further reduced in density relative to  $O$ , thereby enhancing the peak density  $N_m F_2$  by day.

The relationship between  $h_m F_2$  and the vertical plasma drift/meridional wind has been investigated previously, and an approximately linear dependence of  $h_m F_2$  on the meridional wind  $U$  has been found for small winds under steady state conditions (e.g., Hanson and Patterson, 1964). Miller et al. (1986) and Richards (1991) have quantified the  $h_m F_2 \sim U$  relationship using the theoretical Field Line Interhemispheric Plasma (FLIP) model. Similarly, Pavlov and Buonsanto (1997) applied the IZMIRAN model to deduce winds from  $h_m F_2$ . Alternatively, Rishbeth et al. (1978) developed the “servo” model to describe the wind effects on the  $F_2$ -layer, and Buonsanto et al. (1989) have used this method to compute winds from  $h_m F_2$ . However, the assumption of a stationary ionosphere is not always true, especially from sunrise to noon and for several hours after sunset, and may result in inaccurate wind calculations, as pointed out by Titheridge (1993). Titheridge (1995) then proposed a new technique based upon his theoretical model. There are also other papers that deal with factors affecting the ionospheric  $F_2$ -layer, e.g., Kohl and King (1967), Yagi and Dyson (1985), Miller et al. (1987) (see also Rishbeth and Garriott, 1969, and references therein).

The Japanese Middle and Upper atmosphere (MU) radar, located at Shigaraki (34.85°N, 136.1°E), is capable of detecting the incoherent scatter (IS) from the free electrons in the ionosphere. Observations from this radar have been reviewed by Rishbeth and Fukao (1995) regarding thermospheric and ionospheric behavior, and by Fukao et al. (1996) regarding the dynamical features. In particular, Oliver et al. (1990) presented the first MU radar wind results, obtained from summer 1987 until winter 1988, basically a period of low solar activity. Of particular interest, they found that the amplitudes of the winds were generally smaller than those reported elsewhere by a factor of 1.5–2. Igi et al. (1996) calculated winds from  $h_m F_2$  measurements obtained with ionosonde at nearby Kokubunji using the FLIP model and confirmed the results given by Oliver et al. (1990). We note that their calculations were limited to the 1986–1988 period.

In this study we present  $h_m F_2$  results obtained with the MU radar for the period 1986–1995 and compare them with those obtained from the Kokubunji iono-

sonde and the IRI model. The inter-comparison of these  $h_m F_2$  values is interesting, as  $h_m F_2$  provides useful information from which the meridional winds may be deduced. Also given are the ionospheric drift measurements (field-aligned and perpendicular north) and the corresponding winds for the same period. The main purpose of this study is to determine the seasonal and solar activity dependences of  $h_m F_2$ . A theoretical model is used, in combination with the drift measurements, to reveal numerically the relative importance of the neutral wind and electromagnetic drift, and of temperature and neutral composition, for the peak height variation. We first give a brief description of the MU radar IS measurements, then present the measured  $h_m F_2$  and drift velocities and discuss the model results. Finally, we summarize the main content of this study.

## 2. MU radar IS observations

Detailed descriptions of the MU radar IS measurements have been given by Sato et al. (1989), who describe the radar capabilities and make comparisons with other IS radars, and by Fukao et al. (1990), who report later improvements for ionospheric temperature and drift velocity measurements.

$F$ -layer drift measurements are made with a 1-h cycle. In the first 15 min, the radar measures power profiles with 9.6-km range resolution, and then it is assigned to a 45-min drift velocity observation with range resolution of 38.4 km. The 15-min power data are integrated to obtain a single average, and so are the 45-min velocity data. The radar beam is switched sequentially to geomagnetic north, east, south and west at 20° zenith angle each interpulse period. The four power profiles are averaged to yield a single profile. The vector drift velocity (field-parallel and field-perpendicular components) are determined from the appropriate combinations of the four line-of-sight Doppler velocities. The accuracy of the velocity is 5–10 m/s for average daytime ionospheric densities and 1-h integration. To improve the statistical accuracy, we have averaged the drifts over the altitude range 220–450 km for cases of high solar activity and over 220–350 km for cases of low solar activity. This is a crude attempt to keep the range of averaging somewhat centered on the layer peak, in consideration that  $h_m F_2$  increases as solar activity increases.

In order to determine the electron density  $N_e$  from the received power, we apply the seasonal averages of the plasma temperature ratio  $T_r = T_e/T_i$  measured by the MU radar for high and low solar activity (Otsuka et al., 1998).

### 3. Results and discussion

The data used cover the period from summer 1986 until winter 1995. These ten years had average sunspot numbers of 13, 29, 100, 158, 143, 146, 94, 55, 30 and 18, respectively. For the  $N_e$  data, 6667 hourly values for 400 days are used; for drift data, 3821 hourly values for 316 days are used. They are classified according to solar activity and season, i.e., 1986, 1987, 1994 and 1995 are low solar activity, 1989, 1990 and 1991 are high solar activity; January, February, November and December are winter, May through August are summer, and other months are equinox. The number of hourly data points used for averaging for a given season and solar activity is shown in Figs. 1–6.

In this study, we have not grouped data according to geomagnetic activity, which may affect the atmospheric circulation and the electromagnetic drift and therefore  $h_mF_2$ . We expect to focus on the geomagnetic effects in a future work. We note that about 67%  $N_e$  data and 66% drift data are from the quiet geomagnetic condition defined as  $Kp \leq 3$ . During the disturbed periods, we found cases of  $h_mF_2$  increases and fluctuations; however, the day-by-day variability may mask the geomagnetic effects on  $h_mF_2$ .

#### 3.1. $h_mF_2$

Figs. 1–3(a,b) give the averaged diurnal variations obtained with the MU radar for both the solar minimum (the lower solid line) and maximum (the higher thick solid line) and standard deviations for each set of data so averaged. The upper panel shows the number of data used for averaging for the solar maximum, and the lower one shows the same for the solar minimum.  $h_mF_2$  values are also deduced, using the Dudeney (1983) formula, from the monthly ionosonde parameters, namely  $f_oF_2$ ,  $M3000F_2$  and  $f_oE$  measured over Kokubunji, a nearby ionosonde station. The monthly  $h_mF_2$  values are then averaged to obtain the seasonal variation for a specific year. The corresponding IRI  $h_mF_2$  values are also calculated, and those diurnal variations are also shown in these plots. Generally, the error in deducing  $h_mF_2$  from the  $M3000F_2$  factor is considered to be around  $\pm 20$  km; an error of about 15 km for the MU radar  $h_mF_2$  is expected, taking into account the radar’s range resolution, and the errors in correcting the  $N_e$  derivation from the signal power for the temperature effects.

The winter results are demonstrated in Fig. 1.  $h_mF_2$  for the solar maximum is found to be 50–80 km higher than for the solar minimum. The day–night difference in  $h_mF_2$  for the solar maximum is less than 50 km and for the solar minimum is more than 80 km. For the

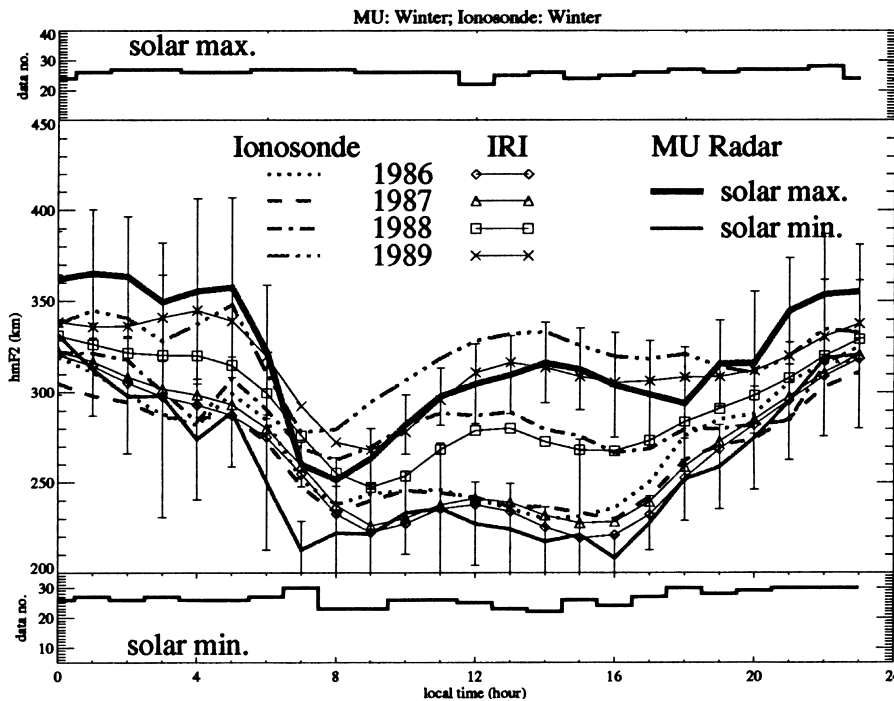


Fig. 1.  $h_mF_2$  diurnal variations for winter observed by the MU radar, and estimated from the ionosonde  $M3000F_2$  and from IRI90. The top and bottom panels show the number of data used for average.

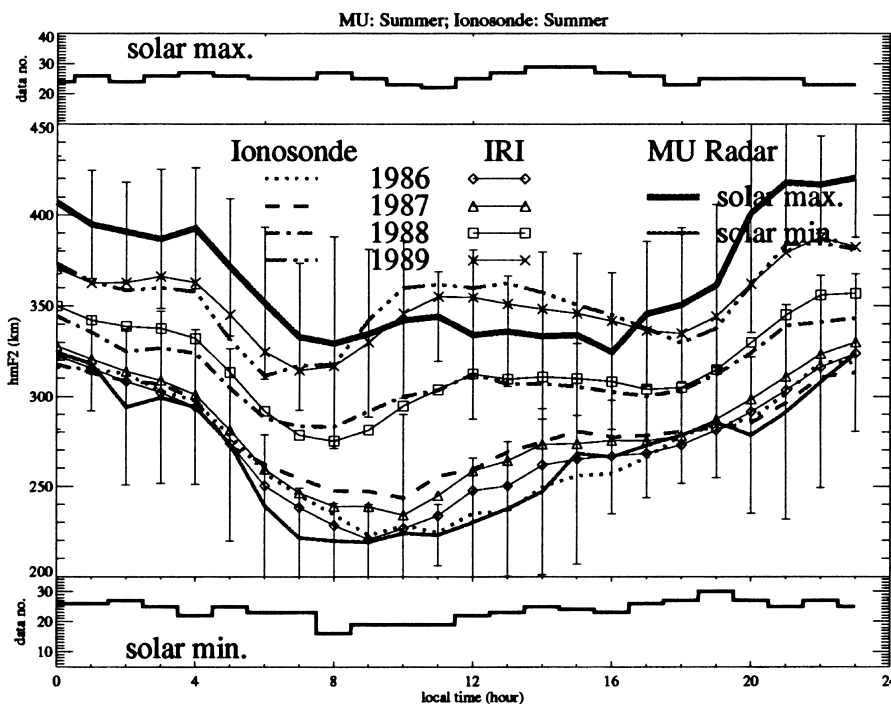


Fig. 2.  $h_mF_2$  diurnal variations for summer observed by the MU radar, and estimated from the ionosonde  $M3000F_2$  and from IRI90. The top and bottom panels show the number of data used for average.

solar maximum,  $h_mF_2$  decreases quickly after sunrise; this decrease is known to be related to the rapid production of ionization in the lower  $F$ -region (Rishbeth and Garriott, 1969).  $h_mF_2$  reaches its lowest value at about 08 LT, then it rises and reaches a daytime maximum around noon or briefly after that.  $h_mF_2$  drops again in the afternoon, reaching a minimum around sunset. The morning drop is more pronounced for the solar maximum while the afternoon drop is more pronounced for the solar minimum. Compared with the ionosonde one, the MU radar  $h_mF_2$  for the solar minimum is 15 km lower during the day, and they are very close to each other during the night. For solar maximum, the MU radar  $h_mF_2$  by day is consistently lower by 20 km than the ionosonde one for 1989, but by night it is higher. The MU radar  $h_mF_2$  is closer to the empirical IRI one than to the ionosonde one; in particular, the MU radar and the IRI  $h_mF_2$  values have very good agreement during the whole day for the solar minimum, and by day for the solar maximum.

Fig. 2 is for summer.  $h_mF_2$  is about 70 km higher for the solar maximum than for the solar minimum.  $h_mF_2$  for the solar maximum reaches minima at 08 and 16 LT, creating a “W”-like diurnal variation as in the winter case. However, for the solar minimum there occurs only the morning minimum, and  $h_mF_2$  steadily increases after the minimum, creating a “V”-like variation. The different behaviors of  $h_mF_2$  diurnal variations,

the “W”- and “V”-like variations, may be related to the differences in  $O^+$  production, the neutral and plasma temperatures, and the neutral wind, as is discussed later. For the solar minimum, the MU radar  $h_mF_2$  exhibits a variation similar to the ionosonde one but is lower by day, approaching the ionosonde  $h_mF_2$  for 1986, and slightly lower by night. For the solar maximum, the MU radar  $h_mF_2$  is lower by day and higher by night. We also note that the IRI  $h_mF_2$  and the ionosonde  $h_mF_2$  are generally in good agreement for each year in Figs. 1 and 2 (except in winter for solar maximum). This might be partly due to the fact that both  $h_mF_2$  values are obtained from the same set of parameters of  $M3000F_2$ ,  $f_0F_2$  and  $f_oE$ . For IRI  $h_mF_2$ , these parameters are calculated from CCIR/URSI coefficients (Bilitza, 1990).

Fig. 3(a) displays the equinox  $h_mF_2$  result. It is more or less in between the summer and the winter  $h_mF_2$  except that, between 10 and 13 LT for the solar minimum and between 12 and 16 LT for the solar maximum,  $h_mF_2$  is largest in equinox indicating a semi-annual variation (see Fig. 3(b) for a summary plot of the MU radar  $h_mF_2$  variations). This type of variation might be due to the effect of the corresponding variations in the atmosphere, which will be addressed later in Section 3.5. In equinox, the peak height drops both in the morning and in the afternoon, and reaches a daytime maximum around noon. The agreements

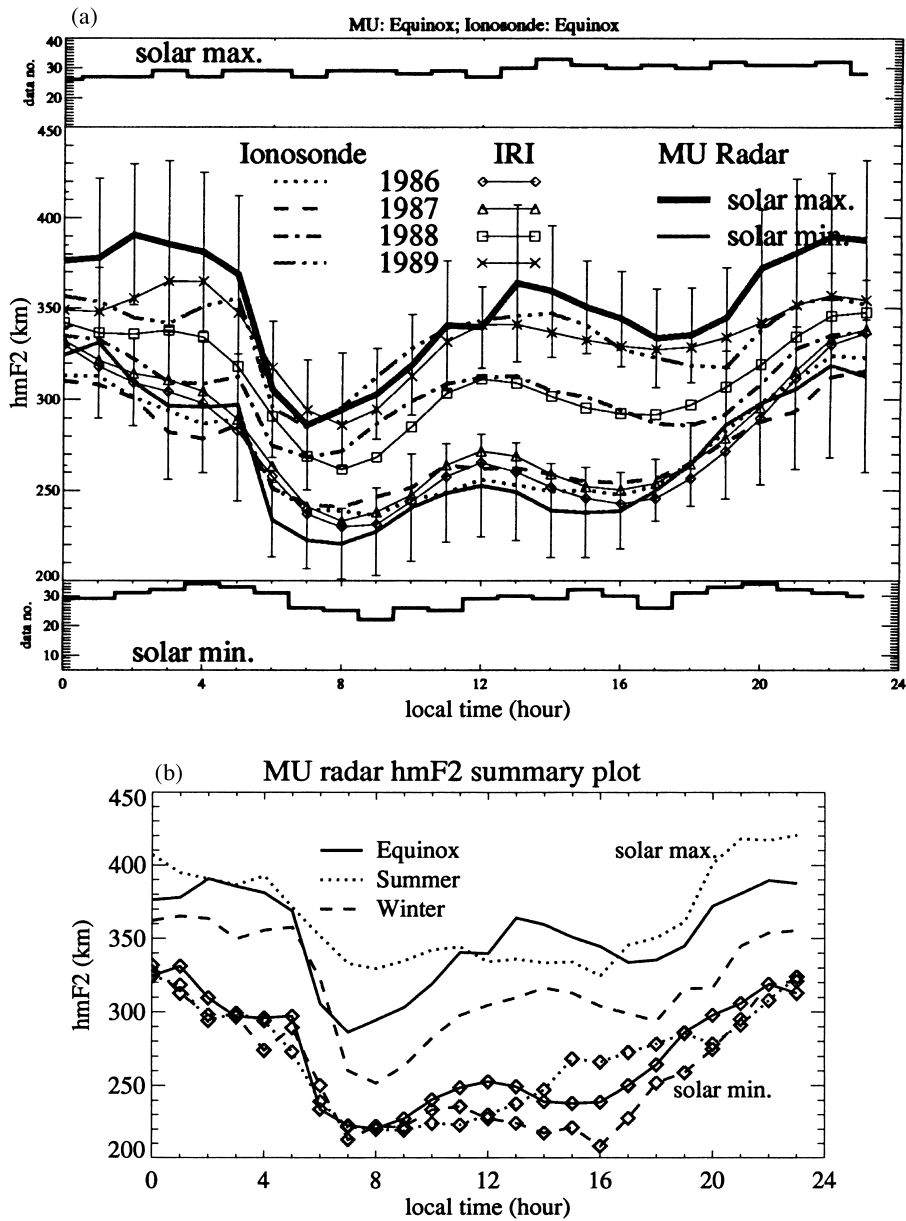


Fig. 3. (a)  $h_m F_2$  diurnal variations for the equinox observed by the MU radar, and estimated from the ionosonde  $M3000F_2$  and from IRI90. The top and bottom panels show the number of data used for average. (b) A summary plot for the MU radar  $h_m F_2$  variations. The upper three curves are for the solar maximum, the lower three curves with diamonds are for the solar minimum.

between the MU radar and the ionosonde data are better during the nighttime for the solar minimum and during the daytime for the solar maximum.

In summary, for the  $h_m F_2$  behavior observed at Shigaraki, we found that: (1)  $h_m F_2$  is generally higher for the solar maximum than for the solar minimum, and higher in summer than in winter; (2) for the solar maximum,  $h_m F_2$  drops markedly in the morning and in the afternoon; however, for the solar minimum, the

$h_m F_2$  minimum occurs in the morning for summer and primarily in the afternoon for winter.

### 3.2. Drift velocities

Figs. 4–6 show the drift measurements averaged over 220–350 km for the solar minimum when the  $F_2$  peak height is low, and over 220–450 km for the solar maximum when the peak is high, for summer, winter

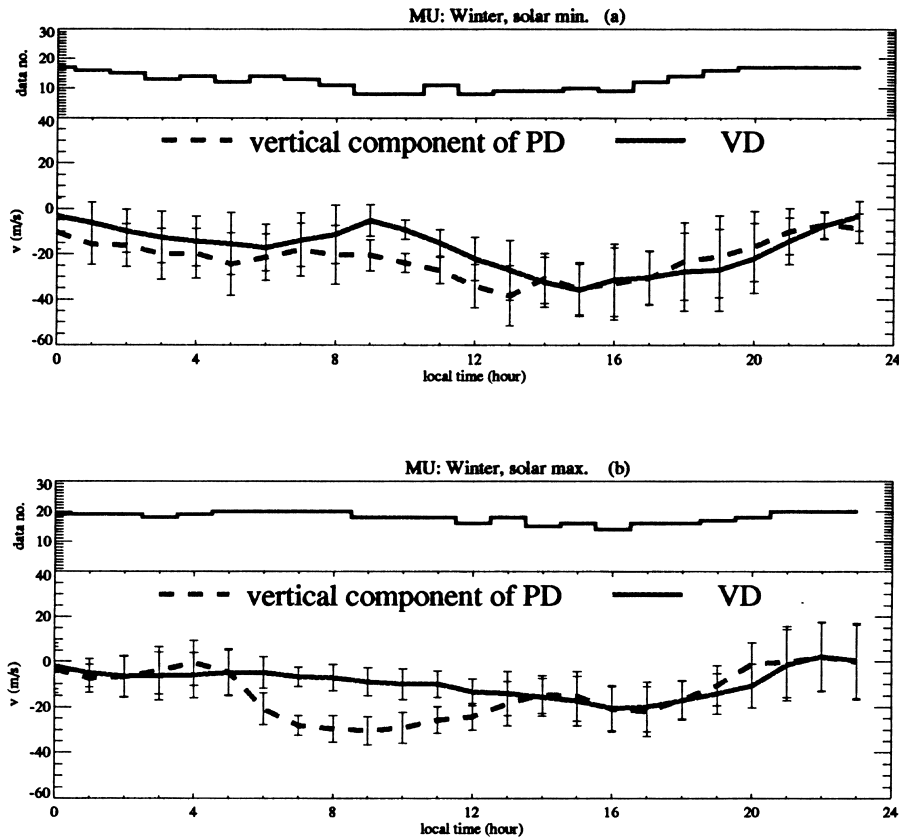


Fig. 4. Diurnal variations of the vertical component of parallel drift (PD) and the vertical drift (VD) for winter as observed by the MU radar. The error bars are obtained from the standard deviation at each hour, and the corresponding number of data used in averaging is shown in the upper panel of each figure. (a) Low solar activity, (b) high solar activity.

and equinox. The parallel drift (PD) includes the contribution of plasma diffusion  $v_d$  and wind-induced drifts  $v_w$  along the magnetic field, and the upward vertical drift (VD) contains contributions from both  $PD = v_d + v_w$  and the northward perpendicular drift  $v_e^N$ :  $VD = PD \sin I + v_e^N \cos I$ .

In winter for the solar minimum (Fig. 4(a)), the vertically downward component of the parallel drift is very small in the morning and reaches a downward minimum around 09 LT. In the afternoon there is a large downward flow; this may be related to a large poleward wind (Fig. 7(a)). The downward vertical drift is smaller than the vertical component of the parallel drift from midnight until 17 LT because of the northward electromagnetic drift. Around sunrise and sunset, the vertical drift speed either decreases or increases smoothly with local time, without any significant jump. For the solar maximum, the parallel drift (Fig. 4(b)), however, presents a maximum downward component in the morning and again in the afternoon, with the morning component being larger. The two maxima correspond to large poleward winds (Fig.

8(a)). The vertical drift, however, does not show a large flow in the morning due to the contribution of electromagnetic drift. In addition, the vertical parallel drift has smaller amplitude for the solar maximum than for the solar minimum.

In summer for the solar minimum (Fig. 5(a)), the downward parallel drift reaches a maximum at 08 and 14 LT. Around sunrise and sunset and near noon the drift tends to be upward. Due to the electromagnetic drift, the overall downward vertical drift is smaller in magnitude in the daytime (05–16 LT) than the vertical component of PD. For the solar maximum (Fig. 5(b)), PD shows a large downward component around 09 and 13 LT, while the northward perpendicular drift during 07–14 LT (for the solar maximum and minimum) leads to a smaller downward vertical drift. The variation of the vertical drift is found to be very small for the solar maximum.

It is noted from the above descriptions that the parallel drift shows larger variation in winter than in summer; the effect of the northward electromagnetic drift tends to cancel out that of the parallel drift on the ver-

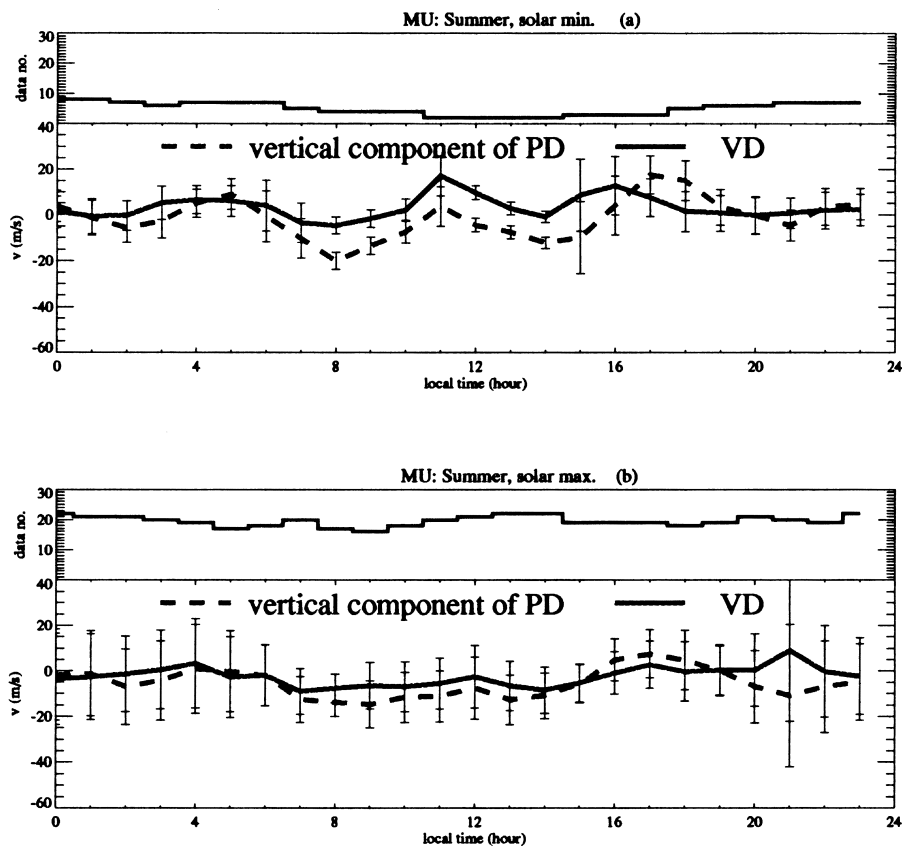


Fig. 5. Diurnal variations of the vertical component of parallel drift (PD) and the vertical drift (VD) for summer as observed by the MU radar. The error bars are obtained from the standard deviation at each hour, and the corresponding number of data used in averaging is shown in the upper panel of each figure. (a) Low solar activity, (b) high solar activity.

tical ion motion. The drift in equinox, as shown in Fig. 6, lies more or less between the summer and the winter drifts.

### 3.3. Modeling results

#### 3.3.1. Model highlights

A theoretical model is used to examine quantitatively the drift and  $h_m F_2$  behavior. The model, developed from our early work (Zhang and Huang, 1995; Zhang et al., 1999), takes account of gravity, pressure gradients and neutral-ion collisions for  $O^+$  and the main photochemical processes for  $O^+$ ,  $NO^+$ ,  $O_2^+$  and  $N_2^+$  over 100–500 km. In order to solve the  $O^+$  diffusion equation, we assume that the lower boundary (100 km) is in photochemical equilibrium, and we set the upper boundary (500 km) electron density to measured values. The neutral concentration and temperature are given by MSIS86 (Hedin, 1987) and the solar fluxes by the EUVAC model (Richards et al., 1994); plasma temperatures are taken from measurement averages (Otsuka et al., 1998). For the  $O^+ - O$

collision frequency we assume a value 1.2 times that of Banks (1966).

In this study, the observed parallel drift is used to constrain the  $O^+$  vertical motion for the model. This has been done by modeling the electron density  $N_e$  for an initial wind (as defined, e.g., by the HWM90 model; Hedin et al., 1991) and then by comparing the model parallel drift with the radar measurements. The differences are then applied to adjust the initial wind so that the next modeling step can in turn minimize the difference. The model drift values are averaged over 220–350 or 220–450 km to keep them consistent with the data. Certainly, the diffusion velocity can vary greatly with altitude, and so such averages may give a result that is not representative of drift at any particular height, but this comparison of drifts between the model and the data is valid, since we treat them in the same way so that no bias arises from averaging one and not the other.

This above procedure of adopting measured parallel drift gives an estimate of the meridional neutral wind. When the model adopts vertical drift measurements,

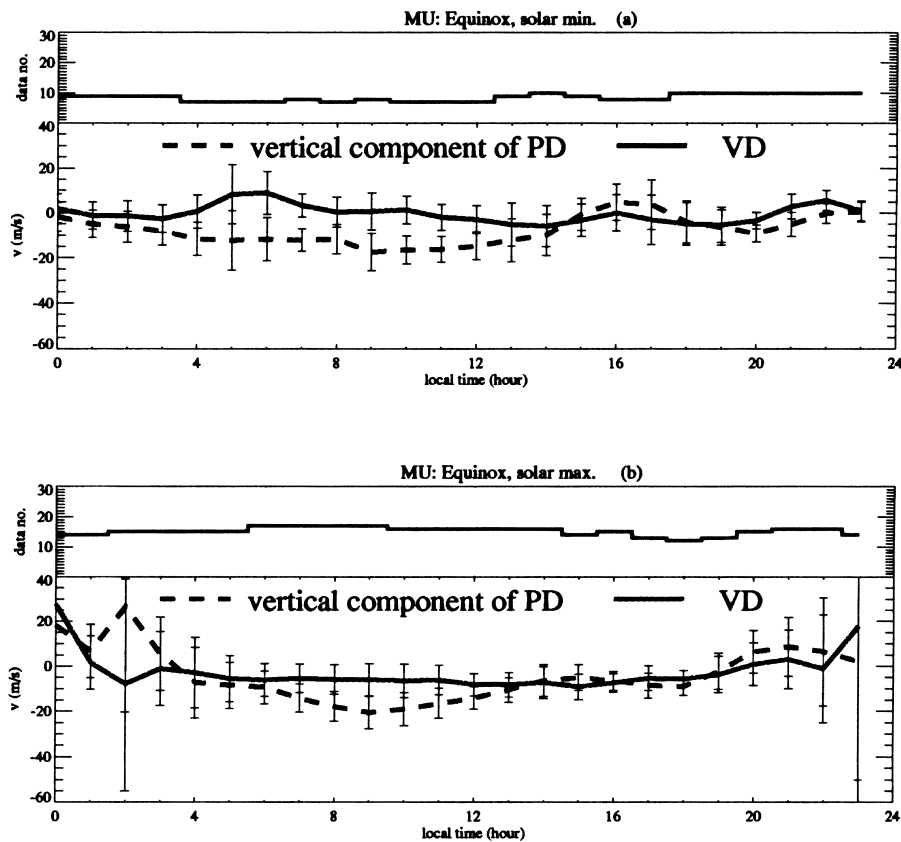


Fig. 6. Diurnal variations of the vertical component of parallel drift (PD) and the vertical drift (VD) for the equinox as observed by the MU radar. The error bars are obtained from the standard deviation at each hour, and the corresponding number of data used in averaging is shown in the upper panel of each figure. (a) Low solar activity, (b) high solar activity.

this procedure gives what may be called an “effective meridional wind”, which includes contributions from both the meridional wind and the drift due to electric fields. The true wind can be obtained by removing the electric-field component. By comparing the results modeled with the parallel and with the vertical drift inputs, we can see the electric field effects.

The calculations are carried out with three diurnal drifts: (1) average diurnal variation; (2) average plus its standard deviation; (3) average minus its standard deviation. The model calculations based on (1) give a set of “average” model values, and on (2) and (3) set “variation limits”, and we will call the spread between these two limits the “variability”. These limits are used to estimate roughly the effects of the variability in the observed drifts on the model  $h_m F_2$  and the neutral wind.

### 3.3.2. The model $h_m F_2$ and the derived neutral wind

The model  $h_m F_2$  results presented in this subsection are obtained with the vertical drift measurements, from which the neutral wind is determined after

removing the perpendicular northward drift and the diffusion velocity.

1. *Winter* (Figs. 7 and 8). The wind in winter exhibits a larger northward component (greater than 50 m/s) by day (Figs. 7(a) and 8(a)). The diurnal mean wind is poleward in winter and equatorward in summer (Figs. 9(a) and 10(a)) for both the solar minimum and maximum. This is associated with the summer-to-winter circulation. The wind variability lies roughly between 20 and 60 m/s for the solar maximum and 20 and 40 m/s for the solar minimum. The variability is larger by night for the solar maximum. For the solar minimum (Fig. 7(a)), the northward wind is particularly large in the afternoon and lowers  $h_m F_2$  (to around 200 km), as can be found in Fig. 7(b). By using the drift observations, our modeling can reproduce quite well the MU radar  $h_m F_2$ . The two large drops of  $h_m F_2$ , in the morning and in the afternoon, seen in the measurements, with the afternoon drop being the larger, are correctly reflected in the modeling.

For the solar maximum (Fig. 8(a)), the meridional

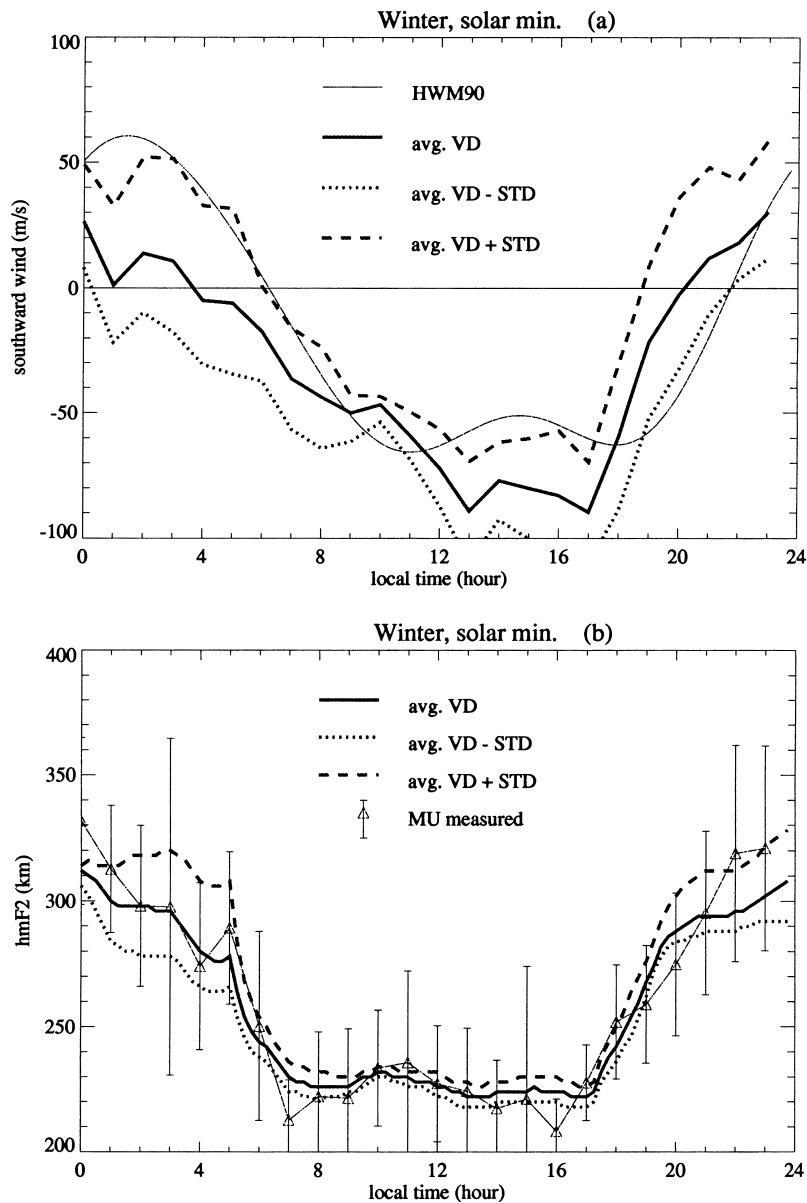


Fig. 7. Model calculations of (a) the southward wind averaged over 220–350 km and (b)  $h_m F_2$  for winter at low solar activity. STD stands for the standard deviation of the averaged (avg.) vertical drift (VD).

wind has a large northward component by day, maximizing in the morning and in the afternoon, with the morning one being the larger. This feature corresponds well to that of  $h_m F_2$ . Modeling with the use of this wind reproduces the “W”-like  $h_m F_2$  variation (Fig. 8(b)). Also, in agreement with the measurements, the drop of the model  $h_m F_2$  is found to be more prominent in the morning than in the afternoon, unlike the situation for the solar minimum.

2. *Summer* (Figs. 9 and 10). The derived wind in

summer for the solar minimum (Fig. 9(a)) is found to be much larger by night than by day. A northward component appears briefly in the morning. The variability is about 50–90 m/s by night and smaller by day. The calculated  $h_m F_2$  (Fig. 9(b)) reveals a large morning drop and a small afternoon drop, similar to the measurement. The measured  $h_m F_2$  is 25 km lower than the model one, probably because the electron density measurement is contaminated below or near the peak by the meteor-echoes for this season. We suppose that the

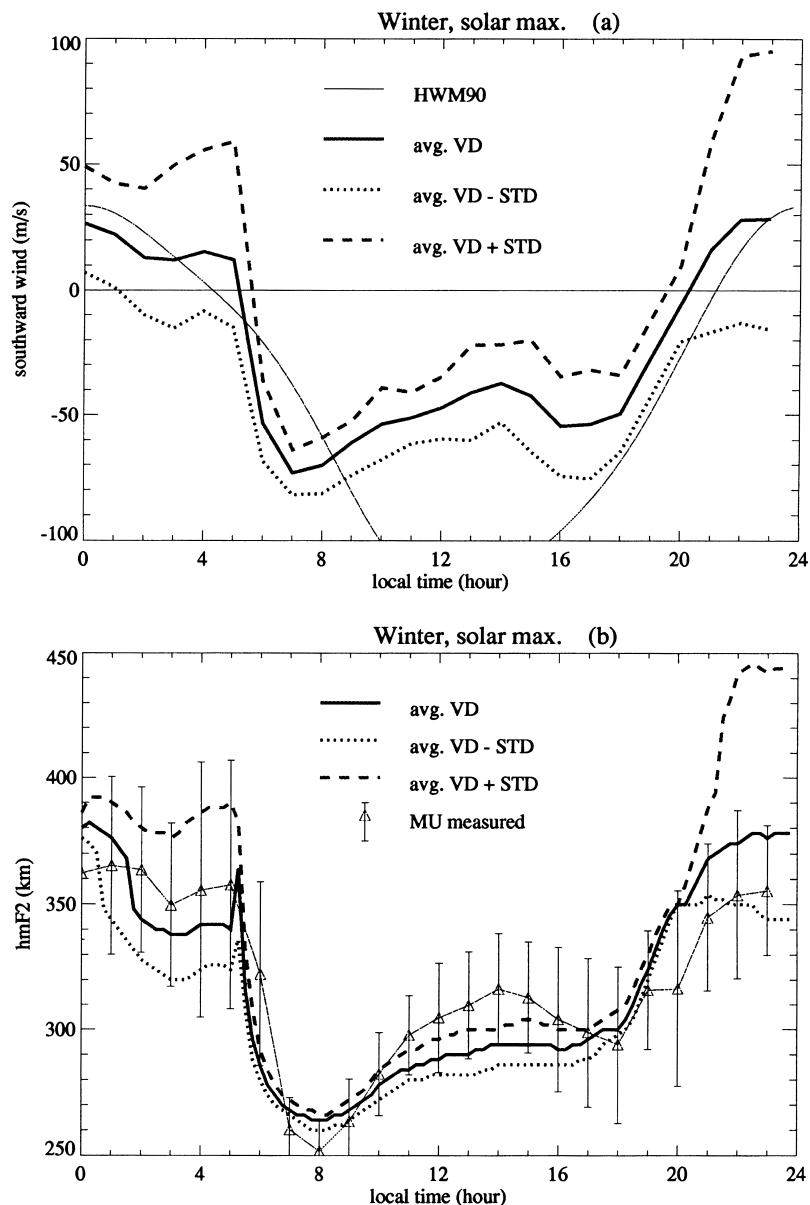


Fig. 8. Model calculations of (a) the southward wind averaged over 220–350 km and (b)  $h_m F_2$  for winter at high solar activity. STD stands for the standard deviation of the averaged (avg.) vertical drift (VD).

ionosonde-based  $h_m F_2$  averaged for summer over 1986 and 1987 may be more representative (the diamonds in Fig. 10(b)).

For the solar maximum, the wind (Fig. 10(a)) is mainly southward by night while by day the northward component is smaller than 20 m/s. The variability of this wind is the largest of all cases, up to 60–110 m/s by night and 30–50 m/s by day. Different from other cases, the daytime wind reaches its maximum speed near noon; however, the calculated  $h_m F_2$  (Fig. 10(b)), in excellent agreement with the

measurement during the whole day, clearly presents two large drops. They seem unassociated with the northward wind but related to other factors which are addressed below.

Comparing the neutral wind derived from the drift data with the empirical wind of HWM90, we find fairly good agreement in summer for the solar maximum, but during the daytime in winter for the solar maximum the agreement is bad for both the wind speed and the shape of its diurnal variation.

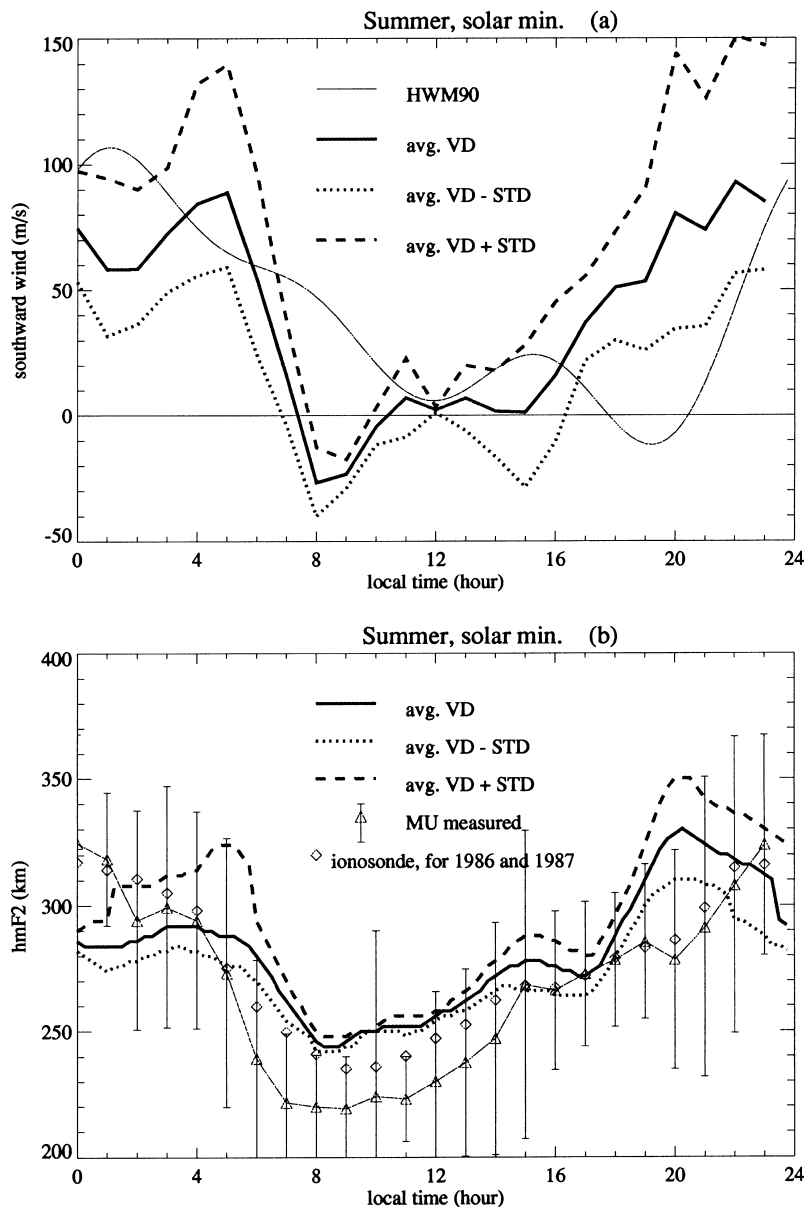


Fig. 9. Model calculations of (a) the southward wind averaged over 220–350 km and (b)  $h_m F_2$  for summer at low solar activity. STD stands for the standard deviation of the averaged (avg.) vertical drift (VD). Also in (b) is the average  $h_m F_2$  for 1986 and 1987 from the ionosonde.

#### 3.4. The wind effects on $h_m F_2$

We have seen the similarity between the wind and  $h_m F_2$  variation patterns, e.g., in winter for the solar maximum condition. To make detailed examinations of the effects of the neutral wind and various other factors on the measurement averages of  $h_m F_2$  obtained during 1986–1995, the following  $h_m F_2$  simulations are carried out under specified neutral wind conditions: (1) zero wind (the dotted lines in Figs. 11–14); (2) aver-

aged wind (i.e., using parallel drift PD; the dashed lines in Figs. 11–14); (3) averaged wind plus northward electromagnetic drift (i.e., using vertical drift VD; the solid lines in Figs. 11–14). The zero-wind calculations produce a so-called “balance height” established by chemical loss and diffusion. The VD calculations, as already obtained in the prior subsection, take into account the electromagnetic drift, while the PD calculations do not. Thus, these simulations will help to determine the relative effects of the wind and electro-

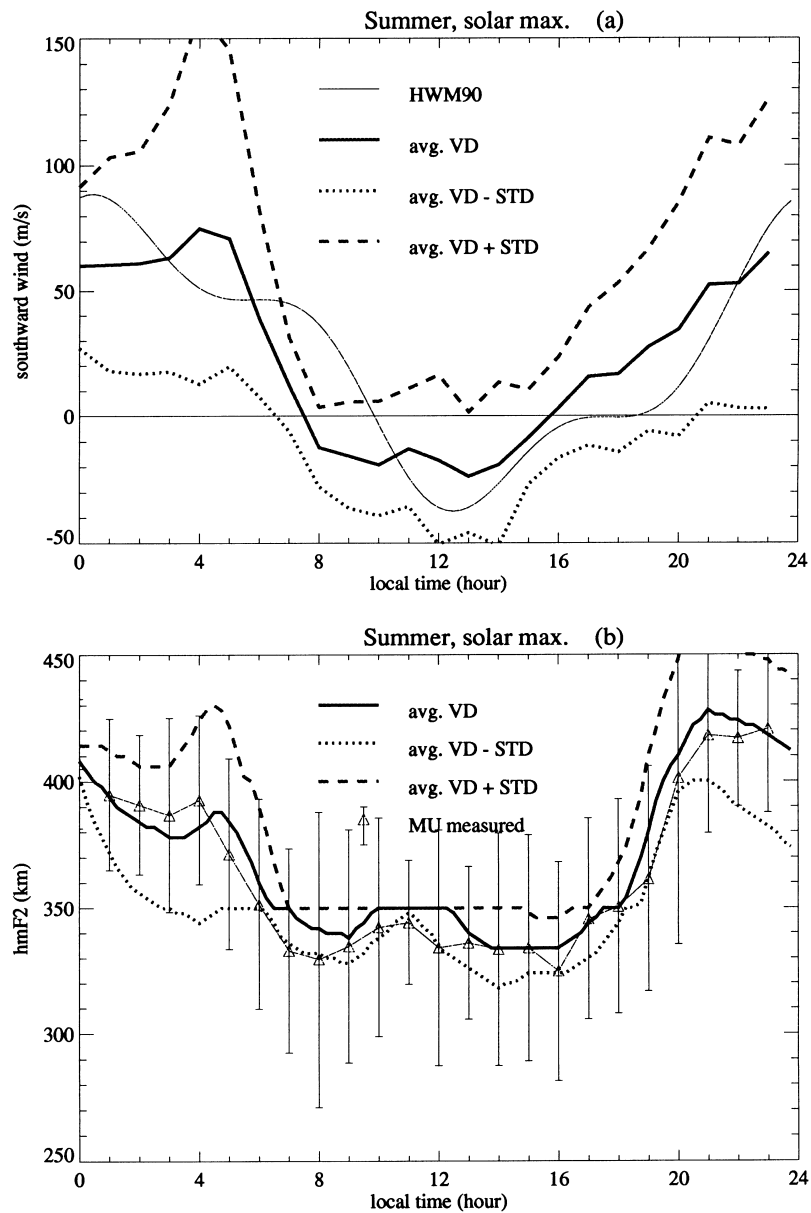


Fig. 10. Model calculations of (a) the southward wind averaged over 220–350 km and (b)  $h_m F_2$  for summer at high solar activity. STD stands for the standard deviation of the averaged (avg.) vertical drift (VD).

magnetic drift, as well as those of chemical loss and diffusion.

1. *Winter* (Figs. 11 and 12). The non-wind peak height for the solar minimum remains constant or increases slightly during the day except for a minor decrease around 16 LT (Fig. 11), while the observed  $h_m F_2$  drops markedly in the afternoon. The daytime neutral wind, strongly northward (compared to that in other seasons and for other levels of solar activity), however, lowers the ioniz-

ation peak by about 20 km from the non-wind peak height, especially in the afternoon when the northward component of the wind is large (see Fig. 9(a)). The effect of the electromagnetic drift is to raise  $h_m F_2$  by less than 10 km before 13 LT, making the  $h_m F_2$  drop in the afternoon still more prominent.

For the solar maximum (Fig. 12), the non-wind peak height drops at 08 and 17 LT. The effect of the wind is to lower the peak height toward the

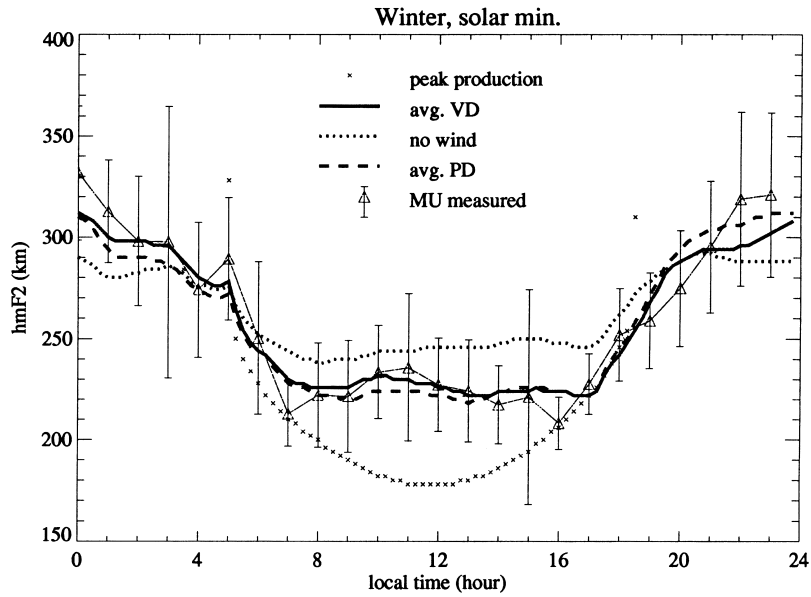


Fig. 11. The calculated  $h_mF_2$  variations with local time for winter at low solar activity for different drift/wind inputs, i.e., without neutral wind; with the averaged (avg.) vertical drift (VD); with the vertical component of the averaged (avg.) parallel drift (PD).

measured level in the morning and in the afternoon. The morning electric field in this case is found to be eastward and has the strongest diurnal variation for any season and solar activity case; thus the northward electromagnetic drift increases the  $F_2$  peak in the morning by more than 10 km, which is the largest electric-field effect of all cases, comparable with

that induced by the neutral wind.

2. *Summer* (Figs. 13 and 14). The wind effect on  $h_mF_2$  is most evident by night, and this nighttime excursion contributes greatly to the day–night difference while the electromagnetic drift effect is relatively less important.

For solar maximum, the non-wind peak height

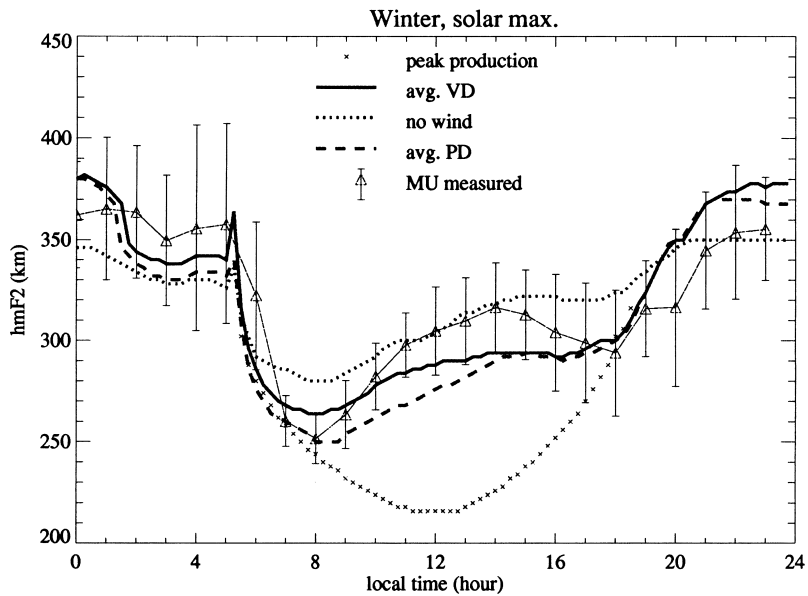


Fig. 12. The calculated  $h_mF_2$  variations with local time for winter at high solar activity for different drift/wind inputs, i.e., without neutral wind; with the averaged (avg.) vertical drift (VD); with the vertical component of the averaged (avg.) parallel drift (PD).

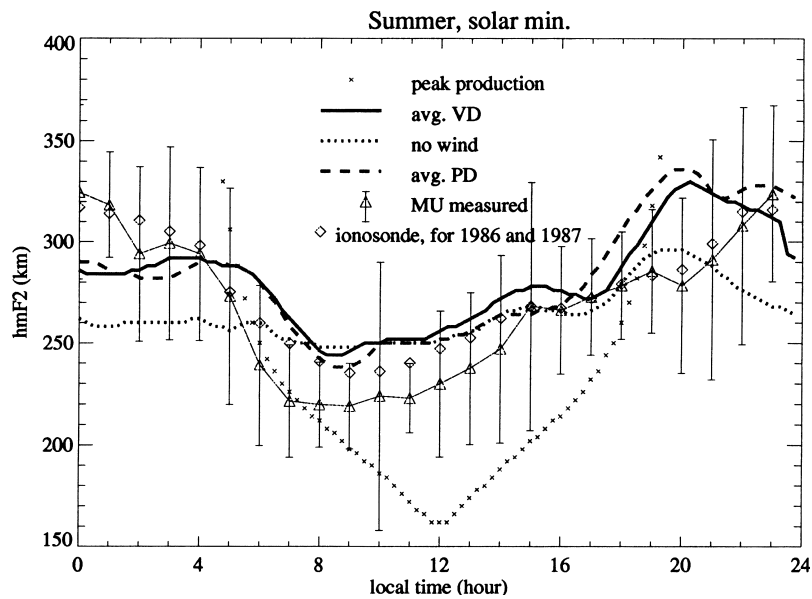


Fig. 13. The calculated  $h_m F_2$  variations with local time for summer at low solar activity for different drift/wind inputs, i.e., without neutral wind; with the averaged (avg.) vertical drift (VD); with the vertical component of the averaged (avg.) parallel drift (PD).

drops in the morning and again in the afternoon; the neutral wind reinforces, more or less, this trend. For the solar minimum, due to the small day–night difference, the non-wind peak height does not show a significant drop but only a slight decrease in the morning. This may be related to the variations of plasma temperature and atmospheric concentrations

since they affect significantly the loss and diffusion processes, as discussed in the next subsection. After sunrise, the observed peak height drops from its nighttime level which was maintained by the southward wind. By day, the meridional wind and the electric field are found to be less important for  $h_m F_2$  behavior.

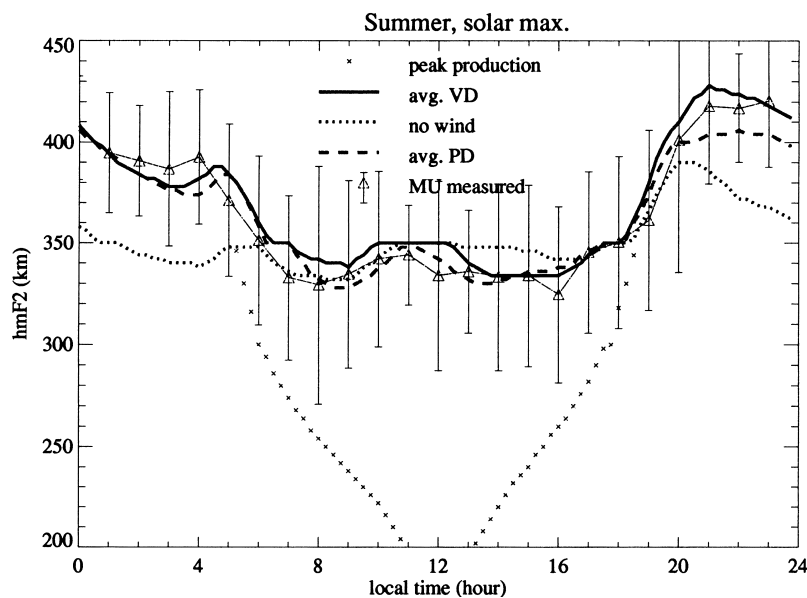


Fig. 14. The calculated  $h_m F_2$  variations with local time for summer at high solar activity for different drift/wind inputs, i.e., without neutral wind; with the averaged (avg.) vertical drift (VD); with the vertical component of the averaged (avg.) parallel drift (PD).

The discussions above indicate that the neutral wind effects on daytime  $h_m F_2$  are evident in winter, particularly at high solar activity, when the meridional wind contains a strong northward component; by night the wind effects become very important in summer. During the day in summer, the northward wind becomes relatively weak and so cannot dominate  $h_m F_2$  behavior; the ionospheric temperatures and neutral composition that control the non-wind peak height then play an important role. The perpendicular northward electromagnetic drift tends to raise the peak height and cancels the wind contribution in the morning. The sudden application of an east–west electric field moves the ionosphere both meridionally and vertically. In time this plasma drift causes a wind which counteracts the vertical motion of the plasma such that the plasma flows horizontally. This process requires  $10^3 \sim 10^4$  s to obtain steady state and so the vertical plasma motions usually do not vanish but remain transient for a few hours. In general, the average electromagnetic drift seems to have only a minor effect on the  $F_2$ -layer for the location of Shigaraki.

### 3.5. Discussion

The height of peak production of  $O^+$  (see the crosses in Figs. 11–14) is higher for high solar activity, because greater neutral atmospheric density increases the optical depth. In the diurnal variation, the height

of peak production decreases toward noon, and the decrease becomes more rapid in summer than in winter due to the solar zenith angle effect.  $h_m F_2$  differs from the height of the peak production because of loss, diffusion and wind effects. We have addressed the wind and electromagnetic effects and mentioned the temperature and composition effects in the section above. These later effects take place as a result of modifications to the loss and diffusion processes that determine the balance height (non-wind peak height).

Time-varying solutions of the “production-loss-diffusion” model by previous authors provided a simple description of the diurnal behavior of the  $F$ -layer (see Rishbeth and Garriott, 1969, and references therein). Now to illustrate details of the effects, we carry out further modeling of the non-wind  $h_m F_2$  by modifying the neutral temperature  $T_n$ , electron and ion temperatures ( $T_e$  and  $T_i$ ) and the neutral composition, as shown in Fig. 15. The calculation is for the summer and the solar maximum condition.

We first simulate the atmospheric thermal expansion effect by increasing  $T_n$  by 500 K in the model neutral temperature. This gives a higher  $h_m F_2$  (the dot–dash line) because of the rise of the height at which  $\beta \sim D/H^2$ , where  $\beta$  is the  $O^+$  loss frequency,  $D$  is the plasma diffusion coefficient and  $H$  is the  $O$  scale height. Therefore, the higher  $T_n$  in the afternoon, creating what is known as the thermospheric density “bulge”, may be responsible in part for the  $h_m F_2$  drop being smaller in the afternoon than in the morning (in the summer for

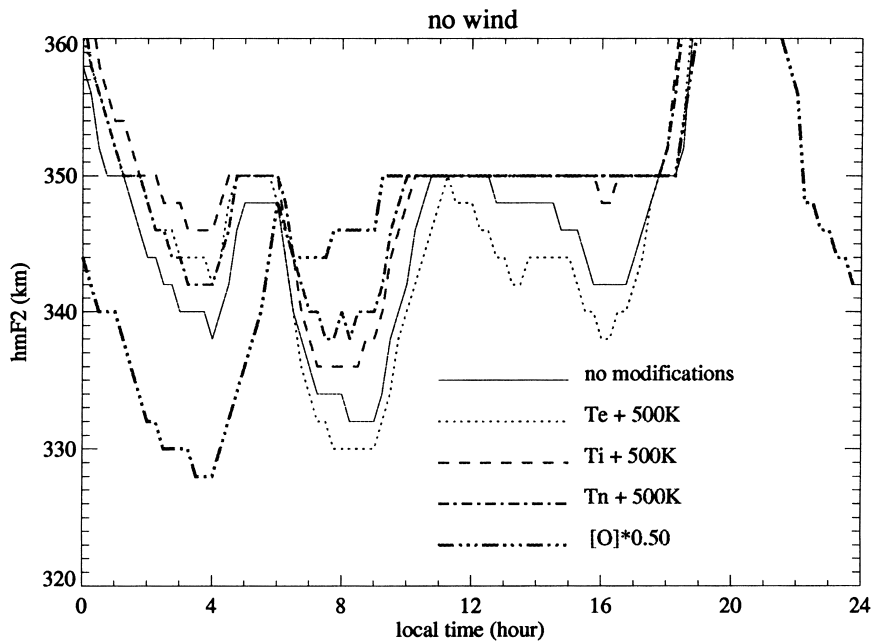


Fig. 15. The balance height (non-wind  $h_m F_2$ ) responses to the changes in the neutral and ionospheric temperatures and in the neutral composition.

the solar minimum). Similarly, the temperature differences for different levels of solar activity may also contribute to the corresponding  $h_m F_2$  difference.  $T_i$  has a similar expansion effect, although it is less efficient than neutral expansion (dashed line) in affecting  $h_m F_2$ .

Increasing  $T_e$  by the same amount of 500 K causes  $h_m F_2$  to increase by night, similar to the  $T_n$  effect. However, by day it lowers  $h_m F_2$  because of the drop of the height at which  $\beta \sim D/H^2$ ; this  $T_e$  effect may partly explain the rapid drop of  $h_m F_2$  in the morning, since the morning enhancement of  $T_e$  is a usual feature explained by photoelectron heating of the low-density electron gas.

As for the composition effect, an atomic oxygen concentration decrease by 50% leads to a significantly enhanced peak height during the day, thus smoothing out the drop of the peak height during the morning and afternoon hours. This is mainly due to reduced  $O^+$  production. By night, the decrease in O concentration results in an increase in the diffusion coefficient and so lowers the height at which  $\beta \sim D/H^2$ . Accordingly, for the solar minimum when the atomic oxygen concentration is not as large as for the solar maximum, the peak altitude will not show dramatic decreases during the day, as can be seen from the  $h_m F_2$  measurements.

#### 4. Summary

This paper has presented the observational results of the height of the maximum ionospheric electron density and the ionospheric drift velocities measured by the MU radar during 1986–1995 at Shigaraki. The ionosonde-based and IRI  $h_m F_2$  values have also been given for comparison. To understand  $h_m F_2$  variation features, its diurnal changes and seasonal and solar activity dependences, a theoretical model has been applied, together with the drift measurements, to determine the relative importance of the meridional wind and northward electromagnetic drift, and of the neutral and plasma temperatures and neutral composition.

It has been found that for the solar minimum there is better agreement between the MU radar and the ionosonde  $h_m F_2$  by night than by day when the former is always lower; for the solar maximum, the MU radar values are higher by night. The agreement is slightly better in equinox. The IRI  $h_m F_2$  is very close to the MU radar  $h_m F_2$  during the whole day for the solar minimum, although slightly higher. For the solar maximum, both  $h_m F_2$  values show agreement by day, but by night IRI underestimates the MU radar  $h_m F_2$  by 20 km or more. In general, the IRI  $h_m F_2$  and the ionosonde one show good consistencies which might be

due to the fact that both  $h_m F_2$  values are estimated from  $M3000F_2$ .

The MU radar data, as well as the ionosonde data and the IRI prediction, show that: (1)  $h_m F_2$  is generally higher for the solar maximum than for the solar minimum, and higher in summer than in winter; (2) for the solar maximum,  $h_m F_2$  drops markedly both in the morning and in the afternoon, while for the solar minimum, the  $h_m F_2$  minimum occurs in the morning for summer and usually in the afternoon for winter. The upward vertical drift tends to be reduced by the electromagnetic drift contribution. The northward winds derived from the observed drifts are found to be very large by day in winter and by night in summer. The variability in the deduced meridional wind is larger by night for the solar maximum.

In general, the measured height of the  $F_2$  peak has been well reproduced using the observed drift velocities, as well as the plasma temperatures, as inputs in the theoretical modeling. This model study shows that the neutral wind contributes greatly to  $h_m F_2$  diurnal variations by lowering the ionization layer by day in winter, and particularly for the solar maximum; it enlarges the day–night difference of  $h_m F_2$  in summer. The northward electromagnetic drift that usually cancels the neutral-wind effect has only a minor effect for the location of Shigaraki. Other features of the observed  $h_m F_2$  variations can be explained basically by the loss and diffusion processes as they are influenced by the temperature and atomic oxygen concentration: the solar maximum–minimum difference of  $h_m F_2$  is due mainly to the neutral temperature difference and the difference in the neutral concentrations that control the height of the peak production; the summer–winter difference of  $h_m F_2$  is also related to the temperature difference and the solar zenith angle difference. The thermospheric “bulge” in the afternoon helps to smooth out the afternoon drop of  $h_m F_2$ . The morning enhancement of the electron temperature may also reinforce the morning drop of  $h_m F_2$ . The daytime drop of  $h_m F_2$  is less dramatic for the solar minimum than for the solar maximum because the lower oxygen concentration for the solar minimum tends to reduce the  $O^+$  production and raise the  $F_2$ -layer in the morning and the afternoon.

#### Acknowledgements

The MU radar belongs to and is operated by the Radio Atmospheric Science Center (RASC) of Kyoto University. One of the authors (S.R.Z.) was supported by the COE program of the Ministry of Education, Science, Sports and Culture of Japan. During the model construction, S.R.Z. obtained support from the

National Natural Science Foundations of China. Another of the authors (W.L.O.) was supported by the National Science Foundation of the United States of America through Grant ATM-9700162. The IRI90 model was kindly provided by Dr D. Bilitza, and the EUVAC, MSIS86 and HWM90 models were obtained from NSSDC, GSFC.

## References

- Banks, P., 1966. Collision frequencies and energy transfer: Ions. *Planetary and Space Science* 14, 1105–1122.
- Bilitza, D. International Reference Ionosphere 1990. National Space Science Data Center/World Data Center A for Rockets and Satellites, 1990. pp. 90–22.
- Buonsanto, M.J., Salah, J.E., Miller, K.L., Oliver, W.L., Burnside, R.G., Richards, P.G., 1989. Observations of neutral circulation at mid-latitude during the equinox transition study. *Journal of Geophysical Research* 94, 987–997.
- Dudeney, J.R., 1983. The accuracy of simple methods for determining the height of the maximum electron concentration of the  $F_2$ -layer from scaled ionospheric characteristics. *Journal of Atmospheric and Terrestrial Physics* 45, 629.
- Fukao, S., Takami, T., Oliver, W.L., 1996. The coupled ionosphere and thermosphere at mid-latitudes in the Asian Sector and its comparison with other locations. *Journal of Geomagnetism and Geoelectricity* 48, 113–124.
- Fukao, S., Sato, T., Tsuda, T., Yamamoto, M., Yamanaka, M.D., Kato, S., 1990. The MU radar: new capabilities and system calibrations. *Radio Science* 25, 477–485.
- Hanson, W.B., Patterson, T.N.L., 1964. The maintenance of the night-time F-layer. *Planetary and Space Science* 12, 979–997.
- Hedin, A.E., 1987. MSIS-86 thermospheric model. *Journal of Geophysical Research* 92, 4649–4662.
- Hedin, A.E., Biondi, M.A., Burnside, R.G., Hernandez, G., Johnson, R.M., Kileen, T.L., et al., 1991. Revised globe model of thermospheric winds using satellite and ground-based observations. *Journal of Geophysical Research* 96, 7657–7688.
- Kohl, H., King, J.W., 1967. Atmospheric winds between 100 and 700 km and their effects on the ionosphere. *Journal of Atmospheric and Terrestrial Physics* 29, 1045–1062.
- Igi, S., Ogawa, T., Oliver, W.L., Fukao, S., 1996. Thermospheric wind over Japan: comparison of ionosonde and radar measurements. *Journal of Geophysical Research* 100, 21,323–21,326.
- Miller, K.L., Salah, J.E., Torr, D.G., 1987. The effect of electric fields on the measurements of meridional neutral winds in the thermosphere. *Annales Geophysicae*, Ser. A 6, 337–342.
- Miller, K.L., Torr, D.T., Richards, P.G., 1986. Meridional winds in the thermosphere derived from measurements of layer height. *Journal of Geophysical Research* 91, 4531–4535.
- Oliver, W.L., Fukao, S., Takami, T., Yamamoto, M., Tsuda, T., Nakamura, Kato, S., 1990. Thermospheric meridional winds measured by the middle and upper atmosphere radar. *Journal of Geophysical Research* 95, 7683–7692.
- Otsuka, Y., Kawamura, S., Balan, N., Fukao, S., Bailey, G.J., 1998. Plasma temperature variations in the ionosphere over the MU radar. *Journal of Geophysical Research* 103, 20,705–20,713.
- Pavlov, A.V., Buonsanto, M.J., 1997. Comparison of model electron densities and temperatures with Millstone Hill observations during undisturbed periods and the geomagnetic storms of 16–23 March and 6–12 April 1990. *Annales Geophysicae* 15, 327–344.
- Richards, P.G., 1991. An improved algorithm for determining neutral winds from the height of the F2 peak electron density. *Journal of Geophysical Research* 96, 17,839–17,846.
- Richards, P.G., Fennelly, J.A., Torr, D.G., 1994. EU-VAC: a solar EUV flux model for aeronomic calculations. *Journal of Geophysical Research* 99, 8981–8992.
- Rishbeth, H., Fukao, S., 1995. A review of MU radar observations of the thermosphere and ionosphere. *Journal of Geomagnetism and Geoelectricity* 47, 621–637.
- Rishbeth, H., Garriott, O.K., 1969. *Introduction to Ionospheric Physics*. Academic Press, New York and London.
- Rishbeth, H., Ganguly, S., Walker, J.C.G., 1978. Field-aligned and field-perpendicular velocities in the ionospheric F2-layer. *Journal of Atmospheric and Terrestrial Physics* 40, 767–784.
- Sato, T., Ito, A., Oliver, W.L., Fukao, S., Tsuda, T., Kato, S., Kumura, I., 1989. Ionospheric incoherent scatter measurements with the middle and upper atmosphere radar: techniques and capability. *Radio Science* 24, 85–98.
- Titheridge, J.E., 1993. Atmospheric winds calculated from diurnal changes in the mid-latitude ionosphere. *Journal of Atmospheric and Terrestrial Physics* 55, 1637–1659.
- Titheridge, J.E., 1995. The calculation of neutral winds from ionospheric data. *Journal of Atmospheric and Terrestrial Physics* 57, 1015–1036.
- Yagi, T., Dyson, P.L., 1985. The influence of neutral temperatures and winds on the F-layer height. *Journal of Atmospheric and Terrestrial Physics* 47, 575–580.
- Zhang, S.-R., Huang, X.-Y., 1995. A numerical study of ionospheric profiles for mid-latitudes. *Annales Geophysicae* 13, 551–557.
- Zhang, S.-R., Fukao, S., Oliver, W.L., 1999. Data modeling and assimilation studies with the MU radar. *Journal of Atmospheric and Solar-Terrestrial Physics* 61, 563–583.